JACS
JOURNAL OF THE AMERICAN CHEMICAL SOCIETY
Article
pubs.acs.org/JACS

Oxygen Atom Transfer and Oxidative Water Incorporation in Cuboidal Mn_3MO_n Complexes Based on Synthetic, Isotopic Labeling, and Computational Studies

Jacob S. Kanady,[§,‡] Jose L. Mendoza-Cortes,[⊥,‡] Emily Y. Tsui,[§] Robert J. Nielsen,[⊥] William A. Goddard, III,*[,⊥] and Theodor Agapie*[,§]

[§]Division of Chemistry and Chemical Engineering , California Institute of Technology, Pasadena, California 91125, United States
[⊥]Materials and Process Simulation Center, California Institute of Technology, Pasadena, California 91125, United States

Supporting Information

ABSTRACT: The oxygen-evolving complex (OEC) of photosystem II contains a Mn_4CaO_n catalytic site, in which reactivity of bridging oxidos is fundamental to OEC function. We synthesized structurally relevant cuboidal Mn_3MO_n complexes (M = Mn, Ca, Sc; n = 3,4) to enable mechanistic studies of reactivity and incorporation of μ_3-oxido moieties. We found that $Mn^{IV}{}_3CaO_4$ and $Mn^{IV}{}_3ScO_4$ were unreactive toward trimethylphosphine (PMe_3). In contrast, our $Mn^{III}{}_2Mn^{IV}{}_2O_4$ cubane reacts with this phosphine within minutes to generate a novel $Mn^{III}{}_4O_3$ partial cubane plus Me_3PO. We used quantum mechanics to investigate the reaction paths for oxygen atom transfer to phosphine from $Mn^{III}{}_2Mn^{IV}{}_2O_4$ and $Mn^{IV}{}_3CaO_4$. We found that the most favorable reaction path leads to partial detachment of the CH_3COO^- ligand, which is energetically feasible only when Mn(III) is present. Experimentally, the lability of metal-bound acetates is greatest for $Mn^{III}{}_2Mn^{IV}{}_2O_4$. These results indicate that even with a strong oxygen atom acceptor, such as PMe_3, the oxygen atom transfer chemistry from Mn_3MO_4 cubanes is controlled by ligand lability, with the $Mn^{IV}{}_3CaO_4$ OEC model being unreactive. The oxidative oxide incorporation into the partial cubane, $Mn^{III}{}_4O_3$, was observed experimentally upon treatment with water, base, and oxidizing equivalents. ^{18}O-labeling experiments provided mechanistic insight into the position of incorporation in the partial cubane structure, consistent with mechanisms involving migration of oxide moieties within the cluster but not consistent with selective incorporation at the site available in the starting species. These results support recent proposals for the mechanism of the OEC, involving oxido migration between distinct positions within the cluster.

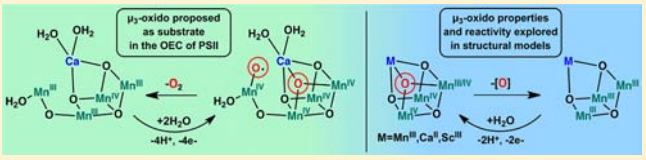

1. INTRODUCTION

Artificial photosynthesis schemes generally involve water as the terminal source of electrons and protons, forming dioxygen as a byproduct.[1] In biological systems, the oxidation of water is performed by the oxygen-evolving center (OEC) of photosystem II (PSII).[2] The OEC consists of a Mn_4Ca cluster supported by bridging oxidos or hydroxidos and carboxylate and histidine side chains from the protein. Early crystallographic, XAS, and EPR studies[3] supported a tetranuclear 3 + 1 arrangement of the four manganese centers, with more recent crystallographic studies proposing a Mn_3CaO_4 heterometallic cubane with a fourth manganese "dangler" bound by a bridging oxide.[4] The exact structure of the cluster remains under debate, with quantum mechanics (QM) studies suggesting that the recent crystal structure corresponds to a more reduced cluster[5] and that a more open structure is more consistent with spectroscopic data.[6]

In the catalytic cycle, or Kok cycle, four photogenerated oxidizing equivalents sequentially oxidize the OEC.[7] Although the oxidation states are still debated,[8] a common assignment of the intermediates, denoted as S_n states (n = 0−4), range in oxidation state from S_0, $Mn^{III}{}_3Mn^{IV}$, to S_4, a putative $Mn^{IV}{}_3Mn^{V}$ or $Mn^{IV}{}_4$-ligand radical that promotes O−O bond formation and O_2 release.[2,9] O−O bond formation has been proposed to involve metal-bound terminal oxo/oxyl, μ_2- or μ_3-oxido moieties (Scheme 1).[2,6,9,10] QM investigations of the mechanism and spectroscopy have been performed in recent years. Quantum mechanics/molecular mechanics (QM/MM) studies support a cubane Mn_3CaO_4 with a Mn dangler arrangement.[9c] A computational comparison of this[9c] and more open structures[11] favors an open-cuboidal arrangement.[10d,11,12] Mechanistic and spectroscopic studies were recently interpreted most consistent with a mechanism of O−O bond formation involving such an open structure (Scheme 1b).[6]

During the catalytic cycle subsequent to O−O bond formation, new substrate water coordinates to the cluster and is deprotonated.[13] For the latter mechanisms (Scheme 1b,c), the water must be deprotonated and incorporated into a μ_3-site, and the cluster must be oxidized. Heterogeneous catalysts for water oxidation based on Ca/Mn mixed oxides displaying structural motifs related to the biological active site have been reported,[14] showing that these elementary reaction steps

Received: October 12, 2012
Published: December 15, 2012

   dx.doi.org/10.1021/ja310022p | J. Am. Chem. Soc. 2013, 135, 1073−1082

Scheme 1. Proposed Mechanisms for O−O Bond Formation at the OEC of PSII (a−c) and Oxygen Atom Transfer and Incorporation Studies Reported Here (d)

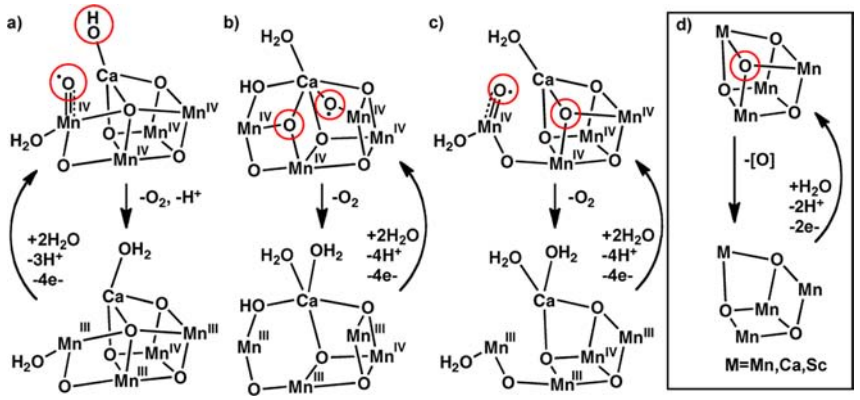

relevant to practical applications. Thus, systematic studies of well-defined model clusters are an important avenue toward uncovering the reactivity of bridging oxido moieties. Additionally, the requisite oxidative incorporation of water as bridging oxido ligands into complex multimetallic structures is key to fully understanding the mechanism of the OEC and heterogeneous metal oxides.

In addition to studies of the complex biological and heterogeneous systems, synthetic metal-oxido models have provided insight into the reactivity and spectroscopy of high-oxidation state manganese clusters.[15] Tetramanganese cubanes have been invoked in water oxidation catalysis,[16] but more recent reports assign the heterogeneous manganese oxide deposited on the electrode as the active electrocatalyst.[17] Although many varieties of tetramanganese-oxido clusters have been characterized,[15] access to structurally related clusters of controlled metal and oxido content able to selectively probe oxygen atom incorporation and transfer has been hindered by challenges related to the method of synthesis by self-assembly. Also, access to calcium-containing manganese clusters was limited to a small number of examples, restricting investigations of the effect of the calcium center.[18] We recently reported a Mn_3CaO_4 cubane supported by a trinucleating ligand and Christou et al. reported a $Mn_3Ca_2O_4$ cluster, both demonstrating that heteronuclear Mn_3CaO_4 cubanes are synthetically attainable.[19]

Utilization of a trinucleating ligand framework, 1,3,5-tris(2-di(2′-pyridyl)hydroxymethylphenyl)benzene (**H_3L**, Scheme 2), has allowed us to prepare a trimanganese complex (**1**) as a useful precursor to site-differentiated manganese-oxido cubanes.[19a,20] Synthetic access to structurally related heteronuclear Mn_3CaO_4 (**4**) and homonuclear Mn_4O_4 (**2**) cubanes has allowed a direct comparison, showing that replacing manganese with calcium leads to a large shift (>1 V) in the reduction potential for accessing a high oxidation state, catalytically relevant, Mn^{IV}_3 species. Given the structural accuracy of these models for the OEC, the chemical reactivities of these and related clusters are of great interest. Herein, we introduce two new complexes: $LMn^{III}_4O_3(OAc)_3$ partial cubane, **3**, and $LMn^{IV}_3ScO_4(OAc)_3(OTf)$ heterometallic cubane, **5**. The series of complexes **2**−**5** enabled us to study the reactivity of μ-oxido moieties, including oxygen atom transfer, oxidative water incorporation, and ligand exchange. Detailed mechanistic understanding was achieved through isotope labeling and electrochemical and QM studies.

2. RESULTS AND DISCUSSION

2.1. Synthesis and Characterization of $LMn_4O_3(OAc)_3$ (3) and $LMn^{IV}_3ScO_4(OAc)_3(OTf)$ (5). We targeted incomplete cubanes for studies of oxygen atom incorporation into elaborate metal oxido clusters. Addition of an equivalent of $Mn(OTf)_2{\cdot}CH_3CN$ and KO_2 (2.5 equiv) to trimanganese complex **1** in THF and stirring for 20 h afforded a red-brown solution. Concentration *in vacuo* and extraction into benzene generated **3** as an orange-red powder (Scheme 2). Compound **3** displays paramagnetically shifted and broadened peaks between 25 and −55 ppm in the ^{1}H NMR spectrum. ESI-MS of the reaction mixture showed peaks at 1241.0 *m*/*z*, $[LMn_4O_3(OAc)_2]^+$, and 1300.1 *m*/*z*, $[LMn_4O_3(OAc)_3]^+$, consistent with a species similar to that of Mn_4O_4 cubane **2** but with one less oxygen. Recrystallization by vapor diffusion of hexane into a THF solution afforded crystals amenable to X-ray diffraction (Figure 1).

Complex **3** displays the ligand coordination mode found in the cubane complexes.[19a] The three basal manganese centers are each square pyramidal and supported by one terminal alkoxide and one pyridyl group from the ligand framework; three pyridyl groups, one per arm, remain unbound. The fourth, apical manganese center is pseudo-octahedral and bound through three κ^2-acetates and three μ_3-oxides to the three basal manganese centers. This arrangement generates a partial cubane missing the "basal" oxido moiety directly above the center of the triarylbenzene motif. Analysis of the Mn−ligand distances and absence of outer-sphere counterions indicate that all metal centers are Mn^{III}. Notably, the incomplete cubane motif Mn_4O_3 has not been isolated previously, although a $[Mn^{III}_3Mn^{IV}O_3L_6]^+$ (L = diphenylphosphinate) species was observed by ESI-MS.[21] Complexes with the $Mn^{III}_3Mn^{IV}O_3X$ formulation, where X is a bridging monoanion (X = Cl^-, I^-, F^-, N_3^-, O_2CR^-, OMe^-, and OH^-) have been studied extensively.[22] The characterization of both **2** and **3**, only differing by an oxygen atom with all ancillary ligands identical, allows a unique opportunity to study systematically oxygen atom transfer from and water incorporation into a cuboidal moiety.

To extend the family of heteronuclear cubanes, we targeted a scandium variant. Treatment of a DMF solution of **4** with scandium triflate and crystallization from acetonitrile/diethyl ether yields the scandium-capped cubane cluster $LScMn^{IV}_3O_4(OAc)_3(OTf)$ (**5**). The ^{1}H NMR spectrum of a CD_2Cl_2 solution of **5** is similar to that of **2**, with paramagneti-

dx.doi.org/10.1021/ja310022p | J. Am. Chem. Soc. 2013, 135, 1073−1082

Scheme 2. Reactivity and Synthesis of Cubanes 2, 4, and 5 and Partial Cubane 3[a]

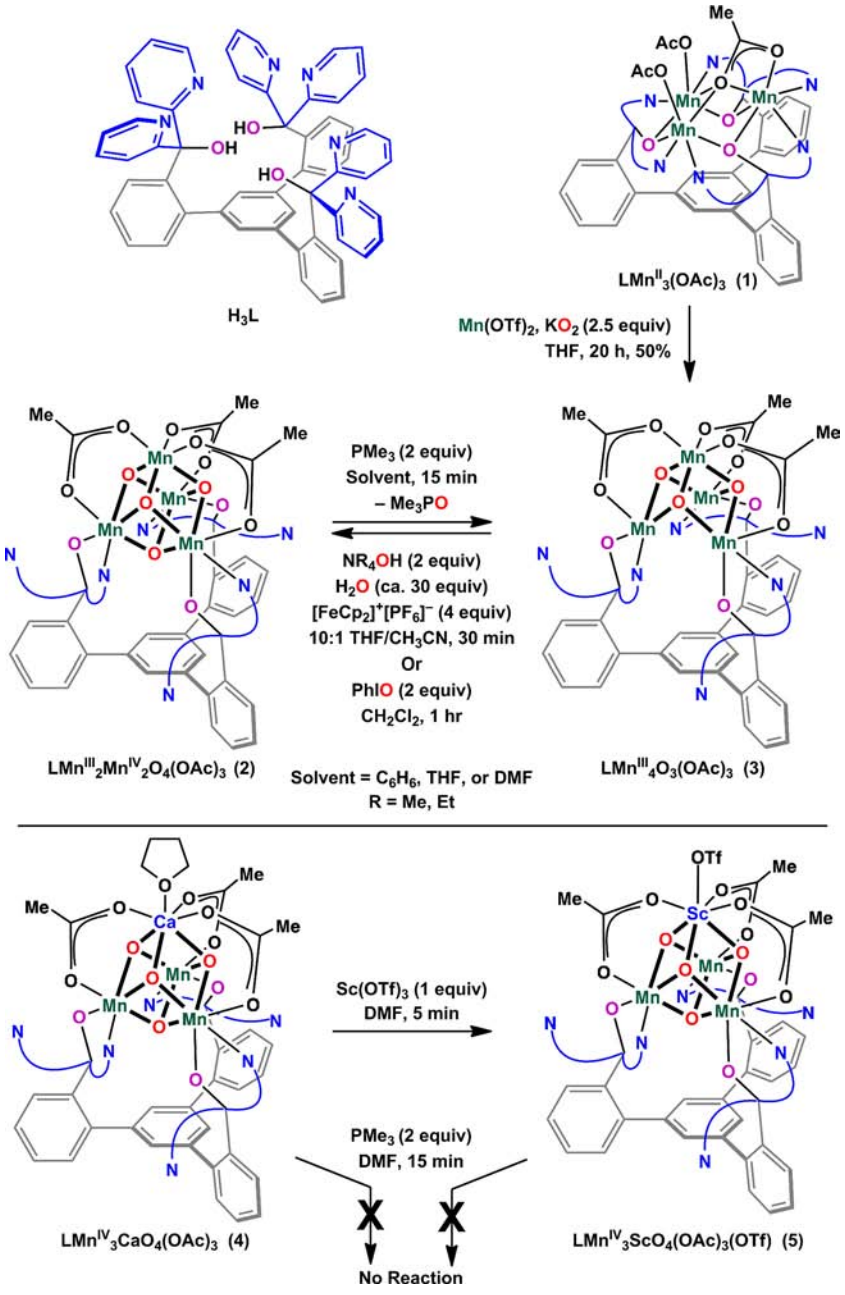

[a]Curved lines represent 2-pyridyl groups.

cally shifted and broadened signals between −24 and 12 ppm. ESI-MS of an acetonitrile solution of **5** showed a single peak at 1306.1 *m*/*z*, $[LScMn_3O_4(OAc)_3]^+$, which is consistent with the assignment of **5**. X-ray quality single crystals of **5** were grown by slow vapor diffusion of diethyl ether into an acetonitrile solution of **5**, and an XRD study of these crystals showed that the solid-state structure of **5** maintains the Mn_3MO_4 cubane core moiety of **4**, but the scandium center is further coordinated by an O-bound triflate anion (Figure 2). The Mn−oxido distances of **5** (1.8477(7)−1.91116(7) Å) are similar to those of **4** (1.825(2)−1.923(2) Å) and consistent with a Mn^{IV}_3 oxidation state assignment.

2.2. O-atom Transfer to Phosphine as Comparative Probe of Mn_3MO_4 Reactivity. With compounds **2**, **4**, and **5** in hand, we investigated the reaction with phosphine as a mechanistic tool, measuring propensity of the oxide for oxygen atom transfer chemistry in these cubanes. Addition of excess (2−10 equiv) trimethylphosphine (PMe_3) to complex **2** produced a color change from red-brown to orange-red. Removal of volatiles *in vacuo* and extraction of Me_3PO with Et_2O afforded **3** as a red-orange powder in near quantitative yield (Scheme 2). In the ^{31}P NMR, ca. 1 equiv of PMe_3 was converted within 15 min with respect to a tetraphenylphosphonium internal standard. The ^{31}P NMR signal corresponding to trimethylphosphine oxide (Me_3PO) was not observed in the reaction mixture of **2** and PMe_3 but could be observed when the PMe_3O was extracted away from the paramagnetic product into diethyl ether (Et_2O). Me_3PO was also observed by ESI-MS of the Et_2O fraction as the Me_3POH^+ cation at *m*/*z* 93.1. The protonated cation mass was also observed for an authentic

dx.doi.org/10.1021/ja310022p | J. Am. Chem. Soc. 2013, 135, 1073−1082

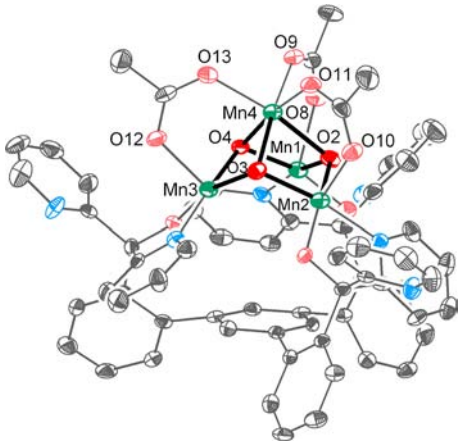

Figure 1. Solid-state structure of complex **3**. Thermal ellipsoids are drawn at 50% probability. Hydrogen atoms and solvent molecules are omitted for clarity. Bolded bonds highlight the Mn_4O_3 core.

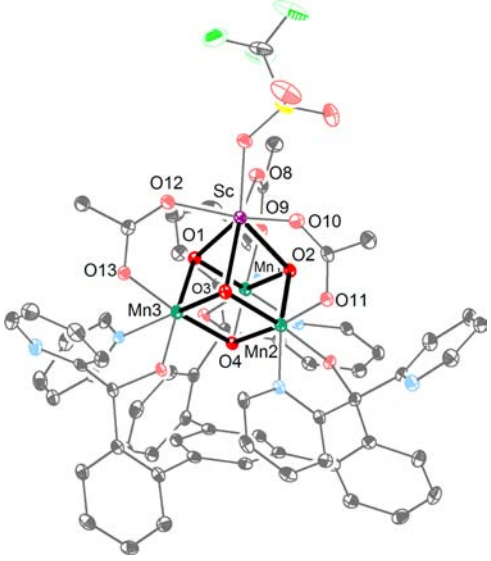

Figure 2. Solid-state structure of complex **5**. Thermal ellipsoids are drawn at 50% probability. Hydrogen atoms and solvent molecules are omitted for clarity. Bolded bonds highlight the Mn_3ScO_4 core.

sample of Me_3PO. Complex **2** also reacts with PEt_3 to give **3**, albeit much slower, 50% conversion over 24 h. In contrast to the fast oxygen atom transfer reaction of **2**, $Mn^{IV}{}_3CaO_4$ and $Mn^{IV}{}_3ScO_4$ cubane complexes **4** and **5** do not show consumption of PMe_3 within fifteen minutes at room temperature (Scheme 2). The calcium-containing cluster **4** (in the same oxidation states as the S_2, S_3, and S_4 state of the OEC)[9c] does not perform oxygen atom transfer to PMe_3, a potent acceptor. The biological system has been interrogated with alternate reducing agents, such as NH_2OH, N_2H_4, and NO, which provided access to reduced forms of the OEC (S_{-n} states).[23] These reagents generate complex mixtures of products with **2**. In contrast, our phosphine surrogate provides clean reductive chemistry and generates a $Mn^{III}{}_4$ complex corresponding to a putative S_{-1} state during OEC photoactivation.[24]

2.2.1. Electrochemistry. The oxidizing power of the clusters was investigated as a measure of oxygen atom transfer propensity. As reported previously, the calcium cluster **4** (E_{red} = −0.94 V vs Fc/Fc^+ in DMA) is less oxidizing than the all-manganese cluster **2** (E_{red} = −0.70 V vs Fc/Fc^+ in DMA).[19a] Cyclic voltammetry experiments revealed that reduction of **5** (E_{red} = −0.24 V vs Fc/Fc^+ in DMF) occurs at a much more positive potential than that of **2** and **4** (Figure 3), indicating

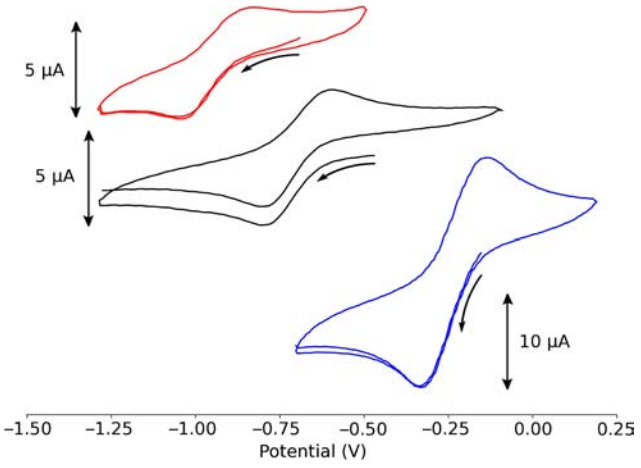

Figure 3. Cyclic voltammograms of **2** (middle), **4** (top), and **5** (bottom) referenced to Fc/Fc^+. The scan rate was 50 mV/s for **2** and 100 mV/s for **4** and **5** at an analyte concentration of 1 mM and electrolyte of 0.1 M $^nBu_4NPF_6$ in dimethylacetamide (**2** and **4**) and DMF (**5**). $E_{1/2}$ values: −0.70 V for **2**, −0.94 V for **4**, −0.24 V for **5**. Open-circuit potentials: −0.47 V for **2**, −0.69 V for **4**, and −0.15 V for **5**. Initial scan direction was negative.

that thermodynamically **5** is more oxidizing. Despite the significantly higher oxidizing power, **5** does not form trimethylphosphine oxide upon treatment with trimethyl phosphine, suggesting that the difference in reactivity is due to the kinetics, which is also consistent with the much slower reactivity of **2** with PEt_3 versus PMe_3.

2.3. QM studies of Oxygen Atom Transfer from Mn_3MO_4 to PMe_3. We carried out QM studies to interrogate the differences in reactivity for oxygen atom transfer to phosphine. As described in the Supporting Information (SI), we used the B3LYP flavor of Density Functional Theory (DFT) with Poisson−Boltzmann solvation.

In order to validate this level of DFT for predicting the structures and properties of these compounds, we compare the XRD coordinates, reduction potentials, and electronic states with the minimized structures obtained from QM. The optimization of the structures was carried out for the high-spin configuration of each compound. Using this structure, we also calculated the lower spin wave functions. We found a very small splitting, <0.1 kcal, for both **2** and **4**, which suggests that the coupling between high-spin manganese centers is a minor contributor to the ambient-temperature free energy surfaces computed (magnetism studies support this small splitting; see SI). For the current level of DFT the difference is too small to be significant, and hence we consider only the high-spin configuration through this discussion.

The QM optimized structure of **4** (147 atoms) is shown in Figure 4a, which differs from the XRD mainly in the THF bound to the Ca, with some small differences in the nonbonded pyridines. Considering only the core Mn_3CaO_4 and the first coordination shell (21 atoms), the DFT differs from the XRD study by root-mean-square (RMS) of 0.007 Å for bonds and 0.384° for bond angles. This indicates that our level of QM reproduces the geometry of **4**.

dx.doi.org/10.1021/ja310022p | J. Am. Chem. Soc. 2013, 135, 1073−1082

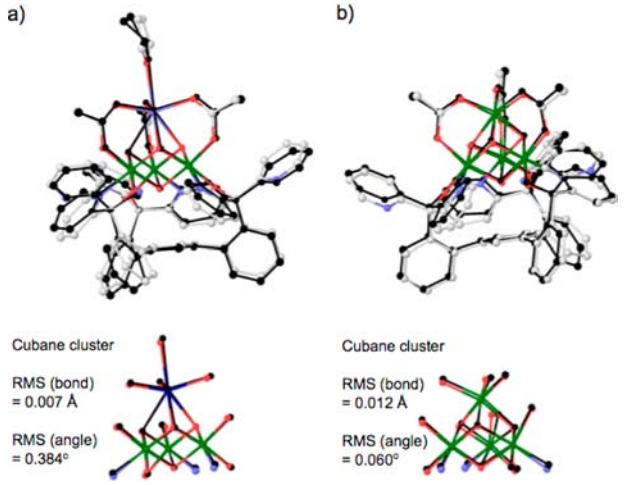

Figure 4. Comparison of geometries of (a) **4** and (b) **2** obtained from experiment (colored: Ca, dark blue; Mn, green; O, red; N, blue; C, gray) and QM (black). H is not shown for clarity.

We then calculated the structure of **2** (134 atoms; Figure 4b) with the main difference involving the nonbonded pyridines with respect to the structure from XRD. Comparing only the Mn_4O_4 cluster and the first coordination shell (20 atoms), the QM agrees with XRD with RMS = 0.012 Å for bonds and 0.060° for angles. Thus again the computational model accurately describes the experimental system for the Mn_4 core.

Using this level of QM, we determined the transition state for the reaction with PMe_3 at various sites of both the Mn_4O_4 and Mn_3CaO_4 clusters. A similar QM study with smaller basis set for geometries was used for other mechanistic studies involving transition-metal complexes in enzymes (including O−O formation), leading to a typical accuracy of within 3−5 kcal/mol of experiment, with the barriers usually overestimated.[25] This difference is systematic not random, giving a potential energy surface similar to the exact one. Also, others have shown that DFT methods are able to reproduce accurately the crystal structures of oxo-manganese complexes.[26]

2.3.1. Distributions of Mn^{III} and Mn^{IV} Sites and Redox Potentials. Comparison of the current QM methodology for single electron redox potentials in well-characterized early transition-metal metallocenes shows an absolute error deviation

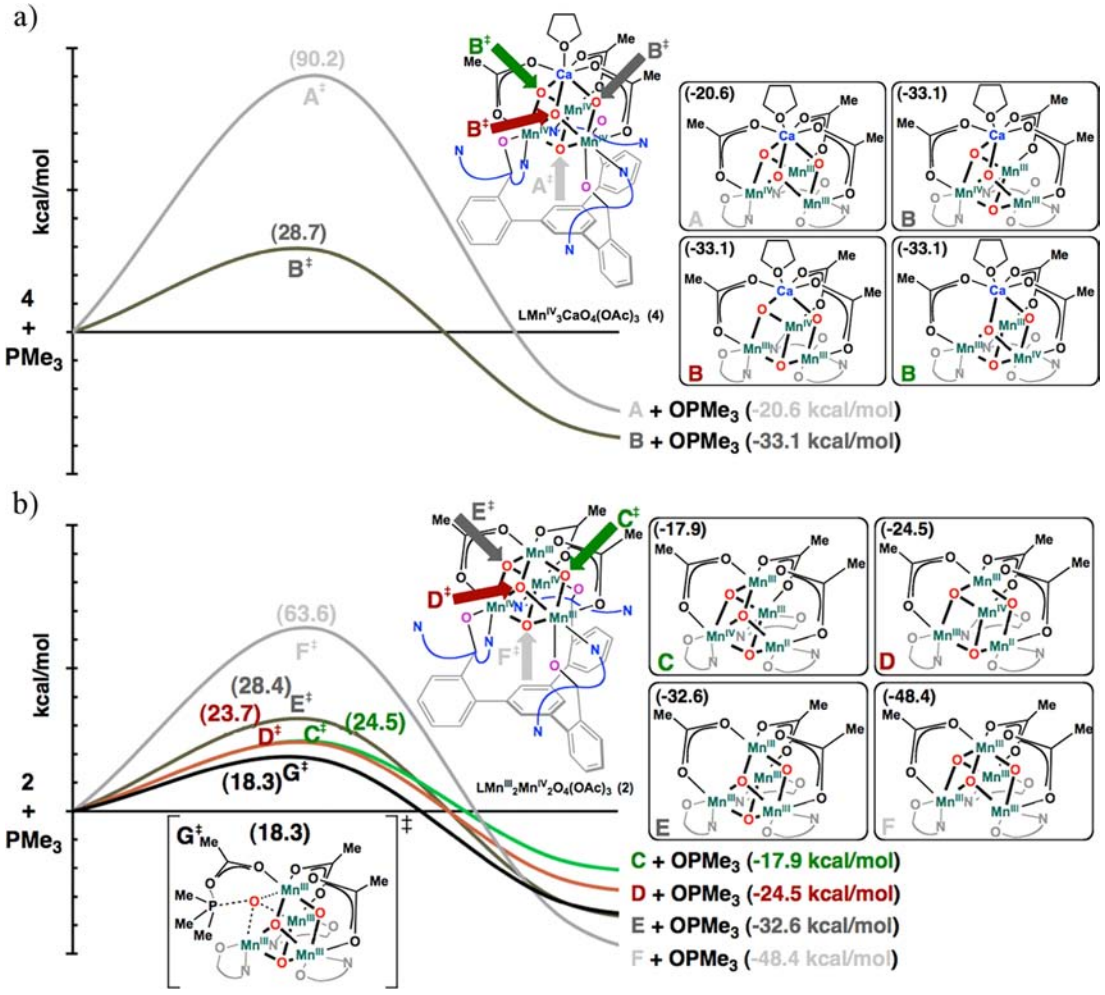

Figure 5. (a) The QM reaction profile of **4** + PMe_3. The possible products **A** and **B** are given in the upper right. The numbers in parentheses are the relative energies with respect to starting materials **4** and PMe_3. (b) The reaction profile of **2** + PMe_3. Transition state $\mathbf{G}^{\ddagger}$ is the transition state found when partial CH_3COO^- detachment is allowed. The possible products **C**−**F** are given in the upper right, with product **F** equivalent to compound **3** isolated experimentally. The numbers in parentheses are the relative energies with respect to starting materials **2** and PMe_3. Boxed structures refer to products, and nonboxed structures refer to transition states.

dx.doi.org/10.1021/ja310022p | J. Am. Chem. Soc. 2013, 135, 1073−1082

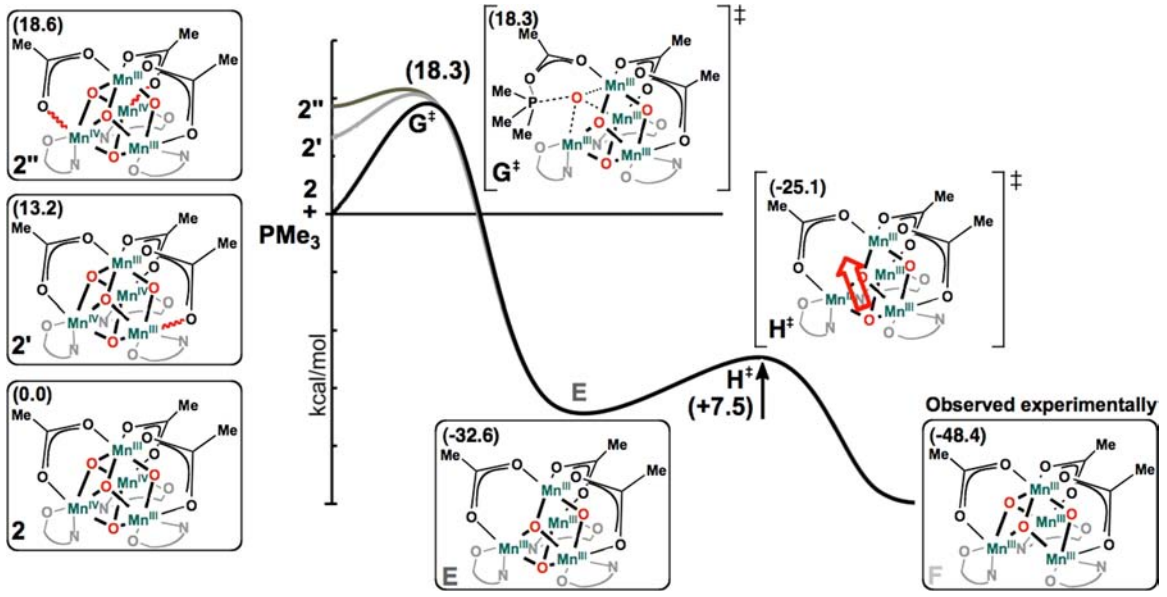

Figure 6. QM-based mechanism proposed for the reaction of PMe_3 and the Mn_4O_4 cubane model **2**.

of 0.179 V. This is equivalent to an error of 4.1 kcal/mol, which is in the range of accuracy for B3LYP (Table S1). The current B3LYP methodology systematically gives more negative potentials than experiment for the Mn_4O_4 and Mn_3CaO_4 cubanes by almost 0.2 V, an error of 4.6 kcal/mol (Table S2). This is similar to the error for single transition-metal complexes in well characterized metallocenes.[27] For each structure optimization of the redox compounds, we used the high-spin state as in the neutral case (see SI). Thus we validated our level of QM by reproducing the experimental redox potential for these systems. We were also able to determine how the redox processes affects the geometry of the structure by reducing the Mn^{IV} atoms to Mn^{III} (see SI).

2.3.2. QM Reaction Profiles for Reaction With PMe_3 to Form $OPMe_3$. 2.3.2.1. PMe_3 Attacking the Mn_3CaO_4. We consider first the reaction profile for PMe_3 attacking the Mn_3CaO_4 compound **4.** We found that reacting away any of the three 'top' oxygens has a barrier of 28.7 kcal/mol while reacting with the 'bottom' oxygen leads to a barrier of 90.2 kcal/mol (pathways $\mathbf{A}^{‡}$ and $\mathbf{B}^{‡}$, respectively; Figure 5a). The attack of 'bottom' oxygen is very unfavorable due to the presence of the trinucleating ligand **L**. Removing a 'top' oxygen gives the most stable product **B**. On the other hand, removing the 'bottom' oxygen leads to a product, **A**, that is 13.2 kcal/mol less stable because the Mn^{IV} is forced to be five coordinate. Also, the O vacancy at the top is likely stabilized by the *trans*-axial alkoxide and pyridine ligands.

2.3.2.2. PMe_3 Attacking the Mn_4O_4. We found that attacking the 'top' oxygens leads to three distinct barriers of 23.7, 24.5, and 28.4 kcal/mol, giving the products **D**, **C**, and **E**, respectively (Figure 5b). These results are very similar to the lowest barrier $\mathbf{B}^{‡}$ (28.7 kcal/mol) of the Mn_3CaO_4 complex. However, for the Mn_4O_4 complex we found a new lower barrier reaction path **G** involving partial detachment of the CH_3COO^-. This new path leads to a transition state $\mathbf{G}^{‡}$ (Figure 5b) with a barrier of 18.3 kcal/mol. This barrier is 5−10 kcal/mol lower than any of the barriers for direct PMe_3 attack on Mn_4O_4 and Mn_3CaO_4. In contrast, reacting with the 'bottom' oxygen gives product **F** (equivalent to the experimentally observed compound **3**) with a high activation barrier $\mathbf{F}^{‡}$ (63.6 kcal/mol) due to the presence of the trinucleating ligand **L**, similar to results for the $CaMn_3O_4$ cubane. We found that **F** (or **3**) is the lowest energy product, consistent with experiment. The products of removing 'top' oxygen atoms are less energetically favorable by 30.5, 23.9, and 15.8 kcal/mol for **C**, **D**, and **E**, respectively, with respect to **F** (Figure 5b). These differences arise because the Mn^{III} centers prefer to have the elongated axis along the empty coordination site and away from the electron-rich alkoxide donors (as is the case for **F**).

Based on these results we propose the following reaction mechanism for oxygen atom transfer from Mn_4O_4 cubane **2** to PMe_3 (Figure 6). First, partial detachment of $CH_3COO{-}Mn^{III}$ and $CH_3COO{-}Mn^{IV}$ involves barriers of 13.2 and 18.6 kcal/mol, respectively. This partial detachment is not observed for the CH_3COO-Mn^{IV} of Mn_3CaO_4 complex **4** because the barrier is 27.1 kcal/mol. That indicates that the $CH_3COO{-}Mn^{III}$ and $CH_3COO{-}Mn^{IV}$ bonds in the Mn_4O_4 system are more labile than in **4**. This leads to the transition-state $\mathbf{G}^{‡}$, giving mainly products **E** and $OPMe_3$ with minor contributions of **C** and **D.** This is followed by migration of the 'bottom' oxygen to a 'top' position with a barrier of 7.5 kcal/mol, leaving behind the vacancy at the bottom which is the product observed experimentally **F** (or **3**).

2.4. Carboxylate Exchange Studies. The difference in the dissociation energies of acetate oxygen from Mn predicted by QM was further explored experimentally by comparison of exchange properties. Solutions of complexes **2**, **4**, and **5** were treated with deuterated acetate ($[n\mathrm{Bu_4N}][CD_3COO]$) in 10:1 THF/CH_3CN, while the incorporation of isotopic label into the complexes was monitored by ESI-MS. In agreement with QM, we found rapid equilibration (<1 min) to a statistical mixture of isotopologues for complex **2**, whereas **4** and **5** did not reach equilibrium within 50 min (Figure S24). These results are consistent with the Mn^{III} sites of **2** being more labile due to electrons in the M−O σ-antibonding orbital, leading to weaker metal−ligand bonds.

2.5. Oxidative Incorporation of H_2O into 3. Incorporation of water into the OEC during turnover is fundamental to the catalysis. Therefore, we studied conversion of partial cubane **3** to **2** to elucidate the mechanism for such oxido-ligand

dx.doi.org/10.1021/ja310022p | J. Am. Chem. Soc. 2013, 135, 1073−1082

incorporation into multinuclear manganese-oxido systems. This transformation corresponds formally to low S-state (S_{-1} to S_1) conversion. The metal oxidation states (Mn^{III} and Mn^{IV}), the nature of the bridging oxido moiety, and the complexity of the cluster are all relevant to the mode of action of the OEC during catalysis. Preliminary studies found that trimethylamine-*N*-oxide, *tert*-butylhydroperoxide, and cumene hydroperoxide did not react with **3** over days, whereas exposure to iodosobenzene generated **2** in 1 h (Scheme 2). Treatment of **3** with a stoichiometric amount of water resulted in no reaction (^{1}H NMR spectroscopy). In the presence of hydroxide and water (ca. 30 equiv H_2O and 2 equiv NR_4OH, R = Me, Et) in THF/CH_3CN, we observed decomposition of complex **3** over hours. Ferrocenium matches the potential window for the oxidation of **3** but not of the desired product, **2** (See Figure S12). Addition of ferrocenium hexafluorophosphate to **3** in the presence of water in THF/CH_3CN (10:1) led to formation of **2** but in low yield and in a mixture with unidentified products. Finally, when we added an excess of ferrocenium hexafluorophosphate (4 equiv) alongside water (20−30 equiv) and hydroxide (2 equiv), we found that **2** was generated as the major product within minutes (Scheme 2). These experiments indicate that both base and oxidant are necessary for incorporation of oxygen from water in this system.

Oxidative incorporation of water has been demonstrated for a dimanganese system; if dissolved in water and exposed to air, a Mn^{III}−(μ-O)−Mn^{III} complex turned into a Mn^{III}−(μ-O)$_2$−Mn^{IV} complex.[28] Also, addition of chloride to a $Mn^{III}{}_4O_2$ 'butterfly' complex facilitated a disproportionation that gave a one-electron oxidized $Mn^{III}{}_3Mn^{IV}O_3Cl$ cubane.[22a] The present protocol mimics the biological incorporation of an oxido ligand into the OEC: water, oxidizing equivalents, and base are all necessary in this two-electron, two-proton process with a tetramanganese cluster. This reaction is important both to OEC turnover and to assembly. Although highly efficient, the OEC must be reassembled frequently under full solar flux due to photooxidative damage to the inorganic cluster and D1 peptide.[29] The process by which the OEC is assembled, called photoactivation,[24] uses Mn^{2+}, Ca^{2+}, Cl^-, bicarbonate, water, and oxidizing equivalents generated by light absorption.[30] Significant advances have defined kinetically distinct species in photoactivation,[31] and the current transformation corresponds conceptually to the putative final steps, the conversion of S_{-1} to S_1.

2.6. Isotopic Labeling Studies of H_2O Incorporation. The above results illustrate a synthetic cycle between Mn_4O_3 **3** and Mn_4O_4 **2** by oxidative incorporation of water and μ_3-oxygen atom transfer. With an understanding of the oxygen atom transfer mechanism (Figure 6), an ^{18}O-labeling study was devised to determine where the water oxygen atom is incorporated into the cluster with respect to the ligand framework (i.e., at one of the three 'top' positions or at the central, 'bottom' position close to the central arene of the ligand). The location of ^{18}O once incorporated provides information about extent of oxido reorganization during water incorporation into these Mn_4O_n systems, which is relevant to the OEC. We interrogated the regiochemistry of incorporation by subsequent oxygen atom abstraction with phosphine and evaluation of ^{18}O/^{16}O distribution in the products.

Labeled base and water ($NMe_4{}^{18}OH$ and $H_2{}^{18}O$) were utilized in the water incorporation conditions (Scheme 3, in box). ESI-MS analysis of the products shows a shift by two units of m/z vs the experiment with natural abundance water

Scheme 3. ^{18}O-Labeling Experiments and Controls[a]

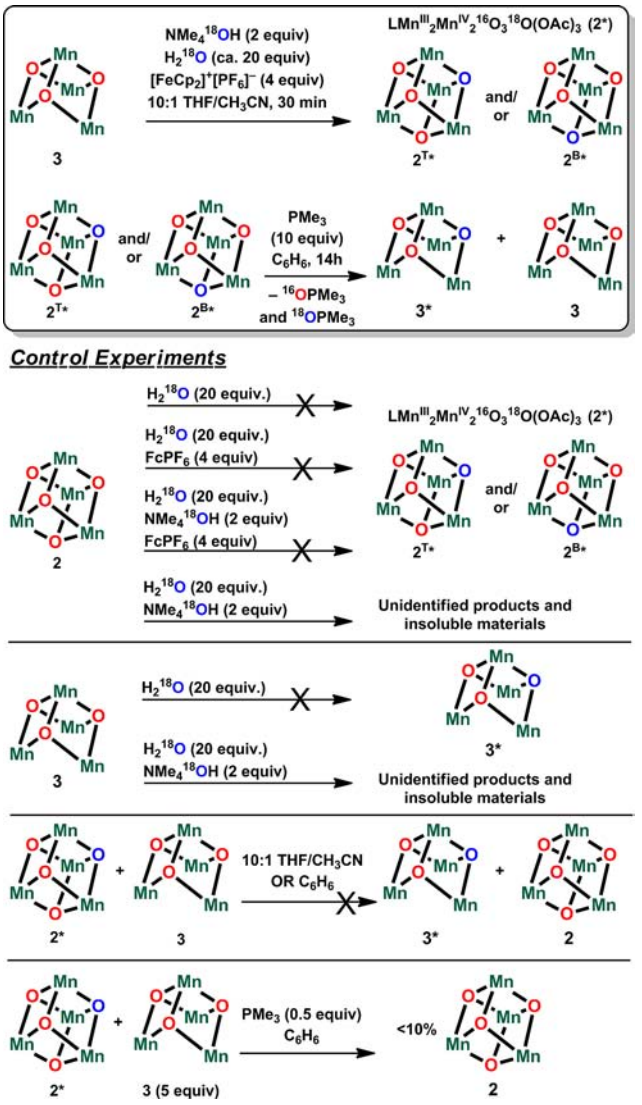

[a]All experiments performed in duplicate or greater. Ligand framework **L** is below Mn_4O_n units as drawn in Scheme 2.

and base (Figure 7a). This indicates generation of the $Mn_4{}^{16}O_3{}^{18}O$ isotopologue, **2***, as the major product in a mixture of higher isotopologues (labeled $\mathbf{2}^{T}$* and $\mathbf{2}^{B}$* in Scheme 3 for ^{18}O incorporation at the "top" and "bottom" positions, respectively); see SI for quantification of isotopologue ratios and ESI-MS data.[32] Higher ^{18}O-content isotopologues of **2*** could form from water exchange in the starting material **3**, product **2**, or from an intermediate species under the oxidizing water incorporation conditions. Control experiments showed no exchange of ^{18}O from water into either **3** or **2** over the time frame of the water incorporation reaction (<1 h; Scheme 3). This is consistent with the slow rate of scrambling in Mn_2O_2 complexes and in another Mn_4O_4 cubane system.[33] We found that complex **2** did not incorporate ^{18}O under the same reaction conditions, showing that the Mn_4O_4 product did not further exchange once fully formed. These experiments taken together suggest that an intermediate species in the conversion of **2** to **3** is responsible for the incorporation of any additional ^{18}O from water. Attempts to isolate intermediate species, for example, a singly oxidized, singly protonated

dx.doi.org/10.1021/ja310022p | J. Am. Chem. Soc. 2013, 135, 1073−1082

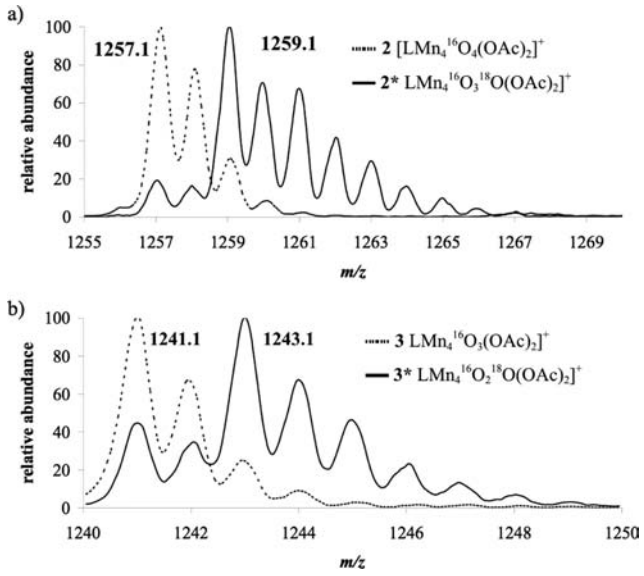

Figure 7. Positive ion ESI mass spectrum of labeled and unlabeled **2** (a) and **3** (b). Both fly as cations with one lost acetate.

$Mn^{III}_3Mn^{IV}O_3(OH)$ species, have been unsuccessful thus far. The Mn_3CaO_4 and Mn_3ScO_4 cubanes **4** and **5** were also subjected to excess $H_2{}^{18}O$ and showed no exchange over 1 h.

Complex **2*** was subjected to an excess of PMe_3 in C_6H_6, producing **3*** as major product in mixture with isotopologues (Figure 7b; Scheme 3).[32a] Labeled $Me_3P^{18}O$ was observed at 95.1 *m/z* along with natural abundance $Me_3P^{16}O$ at 93.1 *m/z* in a ratio of ca. 3:1 $Me_3P^{16}O/Me_3P^{18}O$. To test for the generation of lower nuclearity manganese-oxido species capable of isotopic scrambling, we mixed **3** and **2*** in various solvents and found no isotopic scrambling. Additionally we treated a mixture of **3** (5 equiv) and **2*** with substoichiometric amounts of PMe_3 (0.5 equiv) in benzene to test for lower nuclearity species under oxygen atom transfer conditions. Less than 10% increase of unlabeled **2** was observed by ESI-MS (close to our detection limit). These results are consistent with clusters **2** and **3** being robust in solution supporting the direct oxygen atom transfer from **2** to phosphine, without lower nuclearity intermediates.

We analyzed the isotopologue distribution of **3*** and **3** in the context of various mechanistic possibilities for water incorporation and oxygen atom removal (Scheme 4). In the first step of the study, water could be incorporated at the bottom, the top, or both positions. These incorporation mechanisms give the isotopomers $\mathbf{2}^{\mathbf{B}}$*, $\mathbf{2}^{\mathbf{T}}$*, or a mixture of the two. In the second step—oxygen atom transfer—an oxygen atom could hypothetically be removed from top, bottom, or both sites. These removal mechanisms afford a ratio of **3**/**3*** and $^{18}OPMe_3/^{16}OPMe_3$ that is correlated to the mechanism of the first step: incorporation (Scheme 4, bottom).

The deceivingly simple mechanism of selective ^{18}O incorporation at the bottom position, which is open, followed by selective removal by PMe_3 from the bottom would be consistent with the observed products/starting materials. However this would give solely unlabeled, natural abundance **3** and fully labeled $Me_3P^{18}O$, which is not observed (Scheme 3). If the water were incorporated solely at the top and the bottom oxygen atom was transferred to phosphine, the label location would be opposite: 100% mono-^{18}O labeled **3*** and natural abundance $Me_3P^{16}O$. Because mixtures of **3** and **3*** were observed as well as Me_3PO and $Me_3P^{18}O$, these two

Scheme 4. Mechanistic Possibilities of Water Incorporation and Removal[a]

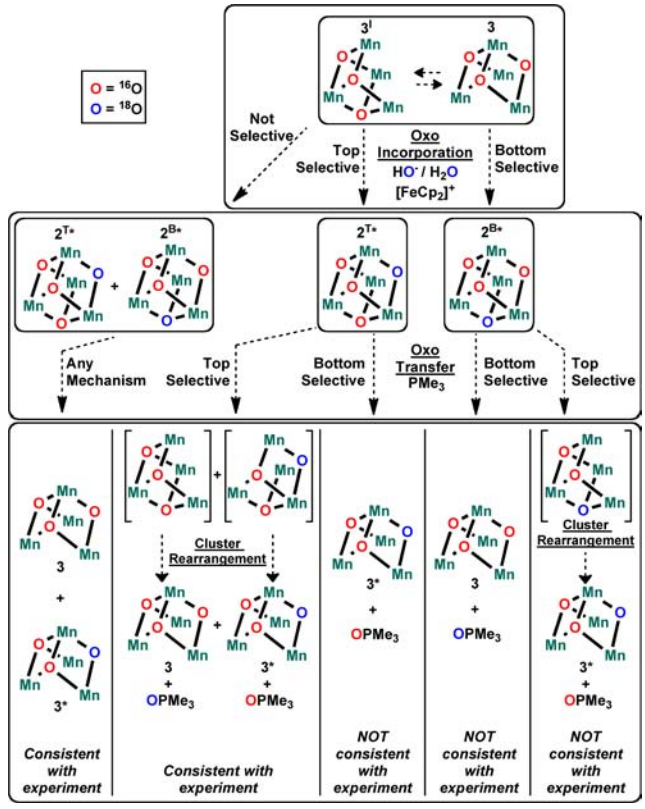

[a]Ligand framework **L** is below Mn_4O_n units as drawn in Scheme 2.

mechanisms can be ruled out, in agreement with the top selective mechanism for oxygen atom transfer to phosphine suggested by the QM studies.[32b] Another mechanism inconsistent with experiment involves water incorporation at the bottom position, followed by selective removal of any of the top three oxidos by PMe_3. This mechanism could be plausible if the lower site were accessible by water and not PMe_3. However, this mechanism would lead to solely **3*** after cluster rearrangement and natural abundance $Me_3P^{16}O$, which again is not observed (Scheme 4, right-hand pathway).[32b]

A number of mechanisms are consistent with the experimental distributions. If water is selectively incorporated into the top positions, $\mathbf{2}^{\mathbf{T}}$* is the sole isotopomer of **2*** formed. Selective transfer from the top oxygen sites would then give a 2:1 mixture of **3***/**3**. If the water incorporation is not selective, then a 3:1 mixture of $\mathbf{2}^{\mathbf{T}}$*/$\mathbf{2}^{\mathbf{B}}$* is expected. Any mechanism of oxygen atom transfer would then give a 3:1 mixture of **3***/**3** (Scheme S1). Both mechanisms are roughly consistent with the experimental ratio of ca. 2:1. Intramolecular scrambling after incorporation also predicts isotopologue mixtures for both **3** and Me_3PO and cannot be distinguished based on the present data.

Given the steric constraints of the ligand framework, the phosphine cannot access directly the bottom oxido of compound **2**, as supported by the high-energy barriers calculated above. Hence, the observed mixture of $Me_3P^{18}O$ and $Me_3P^{16}O$ upon treatment of **2*** with Me_3P suggests that a significant amount of $\mathbf{2}^{\mathbf{T}}$* must be generated upon ^{18}O incorporation from $H_2{}^{18}O$. Isotopomer $\mathbf{2}^{\mathbf{T}}$* may be generated by direct ^{18}O incorporation at the top position upon

dx.doi.org/10.1021/ja310022p | J. Am. Chem. Soc. 2013, 135, 1073−1082

isomerization of **3** to transfer an oxido to the bottom position or migration within $\mathbf{2}^{\mathbf{B}}$*. Either mechanism for ^{18}O incorporation at the top position involves intramolecular migration of oxido moieties in **2** or **3**. Intermolecular versions of this scrambling process are not supported by our control experiments. Hence, although there is more than one mechanism consistent with the present studies, all pathways invoke migration of oxido ligands within the clusters during the process of oxidative water incorporation.

Interestingly, recent computational work suggests that the OEC interconverts between two "sub-state" structures in both the S_1[12b] and S_2 states.[12c] Both studies involve μ-O-migration: a μ_3-oxido or hydroxido bonds more strongly to either a Mn in the cubane subsite or the dangling Mn to form the open-cuboidal structure mentioned above. One report posits that this fluxionality could engender a higher exchange rate to this oxygen consistent with one of the substrate waters as observed in experimental kinetics studies[34] and ^{17}O electron−electron double resonance-detected NMR spectroscopy[6] studies.

3. SUMMARY

Oxygen atom transfer reactivity and incorporation was explored for cuboidal Mn_3MO_n complexes (M = Mn, Ca, Sc; n = 3,4) displaying μ_3-oxido moieties relevant to the OEC in PSII. High-oxidation state heterometallic cubanes $Mn^{IV}{}_3CaO_4$ and $Mn^{IV}{}_3ScO_4$ did not show oxygen atom transfer to trimethylphosphine. In contrast, the $Mn^{III}{}_2Mn^{IV}{}_2O_4$ cubane reacts with this phosphine within minutes to generate a novel $Mn^{III}{}_4O_3$ partial cubane and trimethylphosphine oxide. Reaction paths were interrogated by QM for oxygen atom transfer from $Mn^{III}{}_2Mn^{IV}{}_2O_4$ and $Mn^{IV}{}_3CaO_4$. We found that the preferred mechanism involves partial CH_3COO^- ligand dissociation and coordination with PMe_3. This leads to a five-coordinated phosphorus transition state that is 5−10 kcal/mol lower than when all CH_3COO^- ligands are attached. This partial dissociation of the CH_3COO^- ligand is accessible only when Mn(III) is present. Experimentally, the rate of exchange between metal-bound acetates and CD_3COO^- was highest for $Mn^{III}{}_2Mn^{IV}{}_2O_4$, in agreement with the QM. These results indicate that even with a strong oxygen atom acceptor, such as trimethylphosphine, the oxygen atom transfer chemistry from Mn_3MO_4 cubanes is controlled by ligand lability, with the $Mn^{IV}{}_3CaO_4$ OEC model being unreactive.

The $Mn^{III}{}_4O_3$ partial cubane, **3**, was isolated cleanly upon oxygen atom transfer, without overreduction. This species was converted back to the full cubane $Mn^{III}{}_2Mn^{IV}{}_2O_4$ with water as oxygen source, base, and oxidant, mimicking the biological incorporation of an oxido ligand in the OEC. ^{18}O-labeling experiments were performed via two-step conversions, from $Mn^{III}{}_4O_3$ to $Mn^{III}{}_2Mn^{IV}{}_2O_4$ (with $H_2{}^{18}O$) and back to $Mn^{III}{}_4O_3$ (with phosphine). Following the extent of $^{18}O/^{16}O$ distribution in the products provided mechanistic insight into this two-electron, two-proton process with respect to the position of incorporation into the partial cubane structure. These isotopic labeling experiments support reaction mechanisms involving migration of oxide moieties within the cluster and are not consistent with selective oxide incorporation at the site available in the starting species, thus supporting the possibility of such migration processes during water incorporation into the OEC during photoactivation and turnover. Further studies of multinuclear Mn and Mn/Ca complexes are ongoing toward gaining a better understanding of mechanistic details of oxygen evolution at heteronuclear metal oxide sites such as the one in photosystem II or heterogeneous catalysts.

■ ASSOCIATED CONTENT

Supporting Information

Experimental procedures, characterization data, computational methodology, isotopologue distribution, and crystallographic details. This material is available free of charge via the Internet at http://pubs.acs.org.

■ AUTHOR INFORMATION

Corresponding Author

agapie@caltech.edu; wag@wag.caltech.edu

Author Contributions

‡These authors contributed equally.

Notes

The authors declare no competing financial interest.

■ ACKNOWLEDGMENTS

We are grateful to California Institute of Technology, the Searle Scholars Program (T.A.), the Rose Hill Foundation (J.S.K.), the NSF GRFP (J.S.K. and E.Y.T.), and NSF CHE 1214158 (J.L.M.-C. R.A.N., W.A.G.) for funding. We thank M. W. Day and L. M. Henling for assistance with crystallography and M. Shahgholi for assistance with mass spectrometry. The Bruker KAPPA APEXII X-ray diffractometer was purchased via an NSF CRIF:MU award to Caltech (CHE-0639094) and the computer cluster from NSF-CSEM (DMR-0520565). SQUID data were collected at the Molecular Materials Research Center of the Beckman Institute of the California Institute of Technology.

■ REFERENCES

(1) (a) Gray, H. B. *Nat. Chem.* **2009**, *1*, 7−7. (b) Lewis, N. S.; Nocera, D. G. *Proc. Natl. Acad. Sci. U.S.A.* **2006**, *103*, 15729−15735.

(2) McEvoy, J. P.; Brudvig, G. W. *Chem. Rev.* **2006**, *106*, 4455−4483.

(3) (a) Yano, J.; Kern, J.; Sauer, K.; Latimer, M. J.; Pushkar, Y.; Biesiadka, J.; Loll, B.; Saenger, W.; Messinger, J.; Zouni, A.; Yachandra, V. K. *Science* **2006**, *314*, 821−825. (b) Peloquin, J. M.; Campbell, K. A.; Randall, D. W.; Evanchik, M. A.; Pecoraro, V. L.; Armstrong, W. H.; Britt, R. D. *J. Am. Chem. Soc.* **2000**, *122*, 10926−10942. (c) Zouni, A.; Witt, H. T.; Kern, J.; Fromme, P.; Krauss, N.; Saenger, W.; Orth, P. *Nature* **2001**, *409*, 739−743.

(4) (a) Ferreira, K. N.; Iverson, T. M.; Maghlaoui, K.; Barber, J.; Iwata, S. *Science* **2004**, *303*, 1831−1838. (b) Umena, Y.; Kawakami, K.; Shen, J. R.; Kamiya, N. *Nature* **2011**, *473*, 55−U65.

(5) Luber, S.; Rivalta, I.; Umena, Y.; Kawakami, K.; Shen, J. R.; Kamiya, N.; Brudvig, G. W.; Batista, V. S. *Biochemistry* **2011**, *50*, 6308−6311.

(6) Rapatskiy, L.; Cox, N.; Savitsky, A.; Ames, W. M.; Sander, J.; Nowaczyk, M. M.; Rögner, M.; Boussac, A.; Neese, F.; Messinger, J.; Lubitz, W. *J. Am. Chem. Soc.* **2012**, *134*, 16619−16634.

(7) (a) Joliot, P. *Biochim. Biophys. Acta* **1965**, *102*, 116−134. (b) Kok, B.; Forbush, B.; Mcgloin, M. *Photochem. Photobiol.* **1970**, *11*, 457−475.

(8) Kolling, D. R. J.; Cox, N.; Ananyev, G. M.; Pace, R. J.; Dismukes, G. C. *Biophys. J.* **2012**, *103*, 313−322.

(9) (a) Pecoraro, V. L.; Baldwin, M. J.; Caudle, M. T.; Hsieh, W. Y.; Law, N. A. *Pure Appl. Chem.* **1998**, *70*, 925−929. (b) Pecoraro, V. L.; Hsieh, W. Y. The use of Model Complexes to Elucidate the Structure and Function of Manganese Redox Enzymes. In *Manganese and its Role in Biological Systems*, Sigel, A., Sigel, H., Eds. Marcel Dekker, Inc.: New York, 2000; Vol. *37*, pp 429−504. (c) Sproviero, E. M.; Gascon, J. A.; McEvoy, J. P.; Brudvig, G. W.; Batista, V. S. *J. Am. Chem. Soc.* **2008**, *130*, 3428−3442.

(10) (a) McEvoy, J. P.; Gascon, J. A.; Batista, V. S.; Brudvig, G. W. *Photochem. Photobiol. Sci.* **2005**, *4*, 940−949. (b) Yachandra, V. K.;

Sauer, K.; Klein, M. P. *Chem. Rev.* **1996**, *96*, 2927−2950. (c) Messinger, J. *Phys. Chem. Chem. Phys.* **2004**, *6*, 4764−4771. (d) Siegbahn, P. E. M. *Chem.—Eur. J.* **2008**, *14*, 8290−8302. (e) Siegbahn, P. E. M. *Acc. Chem. Res.* **2009**, *42*, 1871−1880. (f) Siegbahn, P. E. M. *ChemPhysChem* **2011**, *12*, 3274−3280. (g) Siegbahn, P. E. M. *Phys. Chem. Chem. Phys.* **2012**, *14*, 4849−4856.

(11) Ames, W.; Pantazis, D. A.; Krewald, V.; Cox, N.; Messinger, J.; Lubitz, W.; Neese, F. *J. Am. Chem. Soc.* **2011**, *133*, 19743−19757.

(12) (a) Siegbahn, P. E. M. *J. Am. Chem. Soc.* **2009**, *131*, 18238−18239. (b) Kusunoki, M. *J. Photochem. Photobiol., B* **2011**, *104*, 100−110. (c) Pantazis, D. A.; Ames, W.; Cox, N.; Lubitz, W.; Neese, F. *Angew. Chem., Int. Ed.* **2012**, *51*, 9935−9940.

(13) (a) McEvoy, J. P.; Brudvig, G. W. *Phys. Chem. Chem. Phys.* **2004**, *6*, 4754−4763. (b) Haumann, M.; Liebisch, P.; Muller, C.; Barra, M.; Grabolle, M.; Dau, H. *Science* **2005**, *310*, 1019−1021.

(14) (a) Najafpour, M. M.; Ehrenberg, T.; Wiechen, M.; Kurz, P. *Angew. Chem., Int. Ed.* **2010**, *49*, 2233−2237. (b) Shevela, D.; Koroidov, S.; Najafpour, M. M.; Messinger, J.; Kurz, P. *Chem.—Eur. J.* **2011**, *17*, 5414−5422. (c) Zaharieva, I.; Najafpour, M. M.; Wiechen, M.; Haumann, M.; Kurz, P.; Dau, H. *Energy Environ. Sci.* **2011**, *4*, 2400−2408.

(15) (a) Mukhopadhyay, S.; Mandal, S. K.; Bhaduri, S.; Armstrong, W. H. *Chem. Rev.* **2004**, *104*, 3981−4026. (b) Mullins, C. S.; Pecoraro, V. L. *Coord. Chem. Rev.* **2008**, *252*, 416−443.

(16) Brimblecombe, R.; Swiegers, G. F.; Dismukes, G. C.; Spiccia, L. *Angew. Chem., Int. Ed.* **2008**, *47*, 7335−7338.

(17) Hocking, R. K.; Brimblecombe, R.; Chang, L. Y.; Singh, A.; Cheah, M. H.; Glover, C.; Casey, W. H.; Spiccia, L. *Nat. Chem.* **2011**, *3*, 461−466.

(18) (a) Mishra, A.; Wernsdorfer, W.; Abboud, K. A.; Christou, G. *Chem. Commun.* **2005**, 54−56. (b) Hewitt, I. J.; Tang, J. K.; Madhu, N. T.; Clerac, R.; Buth, G.; Anson, C. E.; Powell, A. K. *Chem. Commun.* **2006**, 2650−2652. (c) Kotzabasaki, V.; Siczek, M.; Lis, T.; Milios, C. J. *Inorg. Chem. Commun.* **2011**, *14*, 213−216. (d) Koumousi, E. S.; Mukherjee, S.; Beavers, C. M.; Teat, S. J.; Christou, G.; Stamatatos, T. C. *Chem. Commun.* **2011**, *47*, 11128−11130. (e) Nayak, S.; Nayek, H. P.; Dehnen, S.; Powell, A. K.; Reedijk, J. *Dalton Trans.* **2011**, *40*, 2699−2702. (f) Park, Y. J.; Ziller, J. W.; Borovik, A. S. *J. Am. Chem. Soc.* **2011**, *133*, 9258−2961.

(19) (a) Kanady, J. S.; Tsui, E. Y.; Day, M. W.; Agapie, T. *Science* **2011**, *333*, 733−736. (b) Mukherjee, S.; Stull, J. A.; Yano, J.; Stamatatos, T. C.; Pringouri, K.; Stich, T. A.; Abboud, K. A.; Britt, R. D.; Yachandra, V. K.; Christou, G. *Proc. Natl. Acad. Sci. U.S.A.* **2012**, *109*, 2257−2262.

(20) (a) Tsui, E. Y.; Day, M. W.; Agapie, T. *Angew. Chem., Int. Ed.* **2011**, *50*, 1668−1672. (b) Tsui, E. Y.; Kanady, J. S.; Day, M. W.; Agapie, T. *Chem. Commun.* **2011**, *47*, 4189−4191.

(21) (a) Ruettinger, W.; Ho, D.; Dismukes, G. *Inorg. Chem.* **1999**, *38*, 1036−1037. (b) Ruettinger, W.; Carrell, T.; Baesjou, P.; Boelrijk, A.; Maneiro, M.; Dismukes, G. *J. Inorg. Biochem.* **1999**, *74*, 88−88.

(22) (a) Wang, S. Y.; Folting, K.; Streib, W. E.; Schmitt, E. A.; McCusker, J. K.; Hendrickson, D. N.; Christou, G. *Angew. Chem., Int. Ed.* **1991**, *30*, 305−306. (b) Wang, S. Y.; Tsai, H. L.; Hagen, K. S.; Hendrickson, D. N.; Christou, G. *J. Am. Chem. Soc.* **1994**, *116*, 8376−8377. (c) Aubin, S. M. J.; Wemple, M. W.; Adams, D. M.; Tsai, H. L.; Christou, G.; Hendrickson, D. N. *J. Am. Chem. Soc.* **1996**, *118*, 7746−7754. (d) Aromi, G.; Wemple, M. W.; Aubin, S. J.; Folting, K.; Hendrickson, D. N.; Christou, G. *J. Am. Chem. Soc.* **1998**, *120*, 5850−5851. (e) Aliaga-Alcalde, N.; Edwards, R. S.; Hill, S. O.; Wernsdorfer, W.; Folting, K.; Christou, G. *J. Am. Chem. Soc.* **2004**, *126*, 12503−12516.

(23) (a) Beck, W. F.; Brudvig, G. W. *Biochemistry* **1987**, *26*, 8285−8295. (b) Brudvig, G. W.; Beck, W. F. Oxidation-Reduction and Ligand-Substitution Reactions of The Oxygen-Evolving Center of Photosystem II. In *Manganese Redox Enzymes*; Pecoraro, V. L., Ed.; VCH Publishers, Inc.: New York, 1992; pp 119−140. (c) Messinger, J.; Seaton, G.; Wydrzynski, T.; Wacker, U.; Renger, G. *Biochemistry* **1997**, *36*, 6862−6873. (d) Schansker, G.; Goussias, C.; Petrouleas, V.; Rutherford, A. W. *Biochemistry* **2002**, *41*, 3057−3064.

(24) Cheniae, G. M.; Martin, I. F. *Biochem. Biophys. Res. Commun.* **1967**, *28*, 89−95.

(25) Siegbahn, P. E. M. *J. Biol. Inorg. Chem.* **2006**, *11*, 695−701.

(26) (a) Lundberg, M.; Blomberg, M. R. A.; Siegbahn, P. E. M. *Inorg. Chem.* **2004**, *43*, 264−274. (b) Lundberg, M.; Siegbahn, P. E. M. *J. Comput. Chem.* **2005**, *26*, 661−667. (c) Sproviero, E. M.; Gascon, J. A.; McEvoy, J. P.; Brudvig, G. W.; Batista, V. S. *J. Inorg. Biochem.* **2006**, *100*, 786−800. (d) Orio, M.; Pantazis, D. A.; Petrenko, T.; Neese, F. *Inorg. Chem.* **2009**, *48*, 7251−7260.

(27) Baik, M. H.; Friesner, R. A. *J. Phys. Chem. A* **2002**, *106*, 7407−7412.

(28) Wieghardt, K.; Bossek, U.; Zsolnai, L.; Huttner, G.; Blondin, G.; Girerd, J. J.; Babonneau, F. *J. Chem. Soc., Chem. Commun.* **1987**, 651−653.

(29) Chow, W. S.; Aro, E. M. Photoinactivation and Mechanisms of Recovery. In *The Light-Driven Water: Plastoquinone Oxidoreductase*; Wydrzynski, T. J.; Satoh, K., Eds.; Springer: Dordrecht, 2005; Vol. *22*, pp 627−648.

(30) (a) Miller, A. F.; Brudvig, G. W. *Biochemistry* **1989**, *28*, 8181−8190. (b) Miller, A. F.; Brudvig, G. W. *Biochemistry* **1990**, *29*, 1385−1392. (c) Burnap, R. L. *Phys. Chem. Chem. Phys.* **2004**, *6*, 4803−4809.

(31) (a) Campbell, K. A.; Force, D. A.; Nixon, P. J.; Dole, F.; Diner, B. A.; Britt, R. D. *J. Am. Chem. Soc.* **2000**, *122*, 3754−3761. (b) Tyryshkin, A. M.; Watt, R. K.; Baranov, S. V.; Dasgupta, J.; Hendrich, M. P.; Dismukes, G. C. *Biochemistry* **2006**, *45*, 12876−12889. (c) Dasgupta, J.; Tyryshkin, A. M.; Baranov, S. V.; Dismukes, G. C. *Appl. Magn. Reson.* **2010**, *37*, 137−150. (d) Zaltsman, L.; Ananyev, G. M.; Bruntrager, E.; Dismukes, G. C. *Biochemistry* **1997**, *36*, 8914−8922. (e) Dasgupta, J.; Ananyev, G. M.; Dismukes, G. C. *Coordin. Chem. Rev.* **2008**, *252*, 347−360. (f) Ananyev, G. M.; Dismukes, G. C. *Biochemistry* **1997**, *36*, 11342−11350.

(32) (a) Isotopologue percentages of **2*** (# ^{18}O, %): 0, 9%; 1, 61%; 2, 17%; 3, 9%; 4, 4%; isotopologue percentages of **3***: 0, 28%; 1, 52%; 2, 15%; 3, 5%. (b) Complex **2*** was 9% unlabeled, 61% singly labeled, and 30% higher isotopologues. Higher solvent polarity resulted in increased ^{18}O incorporation: 2:1 THF/CH_3CN rather than 10:1 afforded **2*** with three ^{18}O as the major isotopologue (Figure S22). As a polar solvent was necessary for dissolution of the ferrocenium salt and tetraalkyl hydroxides, some excess ^{18}O incorporation was unavoidable. A 10:1 THF/CH_3CN solvent mixture was utilized throughout the study. Calculations of expected isotope distribution for different mechanisms takes into account the incorporation percentage in **2*** and **3***.

(33) (a) Tagore, R.; Chen, H. Y.; Crabtree, R. H.; Brudvig, G. W. *J. Am. Chem. Soc.* **2006**, *128*, 9457−9465. (b) Ohlin, C. A.; Brimblecombe, R.; Spiccia, L.; Casey, W. H. *Dalton Trans.* **2009**, 5278−5280.

(34) (a) Messinger, J.; Badger, M.; Wydrzynski, T. *Proc. Natl. Acad. Sci. U.S.A.* **1995**, *92*, 3209−3213. (b) Hillier, W.; Messinger, J.; Wydrzynski, T. *Biochemistry* **1998**, *37*, 16908−16914. (c) Hillier, W.; Messinger, J.; Wydrzynski, T. *Photosynthesis: Mechanisms and Effects*; Kluwer Academic Publishers: Dordrecht, 1998; Vol *I*−*V*, pp 1307−1310. (d) Hillier, W.; Wydrzynski, T. *Biochemistry* **2000**, *39*, 4399−4405. (e) Hillier, W.; Wydrzynski, T. *Phys. Chem. Chem. Phys.* **2004**, *6*, 4882−4889. (f) Hillier, W.; Wydrzynski, T. *Coord. Chem. Rev.* **2008**, *252*, 306−317.